Steering Attosecond Electron Wave Packets with Light

R. Kienberger,[1] M. Hentschel,[1] M. Uiberacker,[1] Ch. Spielmann,[1,2] M. Kitzler,[1] A. Scrinzi,[1] M. Wieland,[3] Th. Westerwalbesloh,[4] U. Kleineberg,[4] U. Heinzmann,[4] M. Drescher,[4] F. Krausz[1]*

Photoelectrons excited by extreme ultraviolet or x-ray photons in the presence of a strong laser field generally suffer a spread of their energies due to the absorption and emission of laser photons. We demonstrate that if the emitted electron wave packet is temporally confined to a small fraction of the oscillation period of the interacting light wave, its energy spectrum can be up- or downshifted by many times the laser photon energy without substantial broadening. The light wave can accelerate or decelerate the electron's drift velocity, i.e., steer the electron wave packet like a classical particle. This capability strictly relies on a sub-femtosecond duration of the ionizing x-ray pulse and on its timing to the phase of the light wave with a similar accuracy, offering a simple and potentially single-shot diagnostic tool for attosecond pump-probe spectroscopy.

Interaction of intense laser light with a free electron in the vicinity of an atom has been found to give rise to a series of side bands in the electron energy spectrum (*1*–*4*). The side bands are a manifestation of the absorption and emission of a discrete number of photons by the electron. In the specific case of the free electron arising from photoionization by an extreme ultraviolet or x-ray photon, the electron energies are spread due to simultaneous absorption and emission of laser photons without causing any appreciable change in the electron's average drift velocity (*5*–*7*). We demonstrate that temporal confinement of the photoelectron wave packet to a small fraction of the half wave cycle of the interacting laser light, i.e., to less than 1 femtosecond (1 fs = 10^{-15} s), and its timing to the light phase with similar precision allow light to substantially change the electron's drift velocity.

The temporal structure of the photoelectron wave packet is determined by that of the ionizing radiation. We produce a soft x-ray (henceforth briefly x-ray) burst by high-order harmonic generation in an atomic gas (*8*, *9*) and control its temporal extension by spectral bandpass filtering and by varying the intensity of the few-cycle 750-nm driver laser pulse (pulse duration: τ_L = 7 fs, wave period: T_0 = 2.5 fs). Selecting the highest photon-energy ("cut-off") radiation from the harmonic spectrum results in an isolated sub-femtosecond x-ray pulse (*9*). Using this x-ray pulse to ionize an atomic gas in the presence of a strong few-cycle light field, we demonstrate that the photoelectron spectrum can be up- and downshifted by many times the laser photon energy and by many times the time-averaged oscillatory energy of the electron in the laser field.

The shift of photoelectron energy by up to tens of electronvolts turns into a spread of electron energies over a similar range, if either the duration of the x-ray pulse or its timing jitter becomes comparable to or longer than $T_0/2$, which provides a simple and sensitive attosecond diagnostic tool (*10*, *11*). Our experiments yielded evidence for isolated sub–0.5-fs x-ray pulses emerging with a timing stability to within ±0.2 fs with respect to the phase of the driving light from few-cycle–driven high harmonic generation. The x-ray pulse is found to emerge near the zero transition of the laser electric field. The light-induced energy shift of the photoelectron wave packet excited by this x-ray pulse scales linearly with the instantaneous electric field amplitude up to field strengths in excess of 10^8 V/cm, allowing direct and accurate measurement of the electric field strength of intense laser light as well as monitoring of the stability of the absolute phase of few-cycle light pulses. Previous attosecond time-resolved studies required measurement of electron energy spectra for a number of different delays between the x-ray pump pulse and a visible probe laser (*8*, *9*, *12*). By contrast, the approach presented here provides access to the key characteristics of an attosecond sampling (pump-probe) apparatus consisting of a sub-fs x-ray pulse and a few-cycle visible light pulse (*13*) without any external delay between the two pulses which can be implemented—in principle—in a single laser shot.

[1]Institut für Photonik, Technische Universität Wien, Gusshausstr. 27, A-1040 Wien, Austria. [2]Physikalisches Institut EP1, Universität Würzburg, Am Hubland, D-97074 Würzburg, Germany. [3]Fachhochschule Koblenz, RheinAhrCampus Remagen, Südallee 2, D-53424 Remagen, Germany. [4]Fakultät für Physik, Universität Bielefeld, D-33615 Bielefeld, Germany.

*To whom correspondence should be addressed. E-mail: ferenc.krausz@tuwien.ac.at

Strong Electron-Light Coupling

Energy exchange between light and an electron is most efficient if the electron is moving along the electric field vector of linearly polarized radiation. We studied the electrons emitted in this direction (*11*). In a semiclassical treatment, the electron is detached by absorption of an x-ray photon of energy $\hbar\omega_x$ from an atom and released with an initial energy of $W_0 = m_e v_i^2/2 = \hbar\omega_x - W_b$ in the direction of the electric field $E_L(t) = E_a(t)\cos(\omega_L t + \varphi)$ of the light pulse. Here, ω_x and ω_L stand for the x-ray and light frequency, respectively; W_b is the electron's atomic binding energy; $E_a(t)$ represents the amplitude envelope of the light pulse; and the phase φ adjusts the carrier wave's timing to the envelope, which has been referred to as absolute or carrier-envelope phase.

Solution of the classical equation of motion in the adiabatic limit, $dE_a(t)/dt \ll E_a(t)\omega_L$, and in the dipole approximation (the electron remains localized within a fraction of the wavelength during the interaction) yields the final velocity $v_f = v_i + [eE_a(t_r)/m_e\omega_L]\sin(\omega_L t_r + \varphi)$. Energy gain or loss is maximal for release times at which $E_L(t_r) = 0$, i.e., $\omega_L t_r + \varphi = \pi/2 + m\pi$, resulting in the minimum and maximum final electron energy of $W_f = W_0 + 2U_p(t_r) \pm \Delta W$ for m as an odd or even integer, respectively. Here, $\Delta W = [8W_0U_p(t_r)]^{1/2}$ and $U_p < W_0/2$ has been assumed. Furthermore, $U_p(t_r) = e^2E_a^2(t_r)/4m_e\omega_L^2$ is the electron's quiver energy averaged over an optical cycle and, hence, $\Delta W \propto E_a(t_r)$. If $U_p \ll W_0$, the energy shift is dominated by ΔW and is therefore linearly proportional to the laser electric field strength. For a large initial velocity along the laser polarization ($m_e v_i^2/2 \gg \hbar\omega_L$), this energy gain or loss may far exceed the laser photon energy even for moderate field strengths characterized by $U_p < \hbar\omega_L$. The momentum transfer associated with this energy exchange permits efficient steering of the electron's drift motion (*14*). Why could this light-control of electronic motion not be observed experimentally until now (*15*)? An obvious reason is the lack of sufficiently accurate and reproducible timing of the instant of release to the phase of the light field. If an x-ray pulse with a temporal extension comparable to or longer than T_0 excites the atom, the electron's release cannot be timed to any specific phase of the light field.

We have used a quantum mechanical treatment (*11*) to analyze photoelectron motion in the laser field for ionizing x-ray pulses with durations ranging between $\tau_x > T_0$ and $\tau_x \ll T_0$ and timed to ensure maximum energy gain from the light field in the limit of $\tau_x \ll T_0$ (Fig. 1A). The relevant parameters of the interaction are given in the caption of

Fig. 1. The narrow spectral peaks that are spread over a range of $2\Delta W$ for $\tau_x \geq T_0$ gradually disappear as τ_x, the full width at half maximum (FWHM) of the intensity profile of the wave packet, is shortened to less than $T_0/2$. For $\tau_x < T_0/5$, they turn into a single smooth spectrum upshifted by ΔW. This behavior occurs regardless of whether temporal broadening of the electron wave packet is caused by spectral narrowing or by spectral phase modulation (Fig. 1, B and C, respectively). Strong electron-light coupling (high v_i parallel to E_L) along with sub-$T_0/5$ temporal confinement is predicted to give rise to a striking nonlinear optical effect: low-order transitions (absorption or emission of a single or a few photons) can be completely "switched off" upon simultaneous activation of a high-order transition (Fig. 2). We demonstrate this phenomenon experimentally and address its implications for attosecond metrology.

Controlling the Duration of Photoemission

The temporal extension of the electron wave packet can be affected by shaping the ionizing x-ray pulse. The briefest emission of extreme ultraviolet or x-ray radiation has so far been demonstrated by the generation of high-order harmonics of intense femtosecond light pulses in an atomic gas (*16*, *17*). High-harmonic radiation driven with sub–100-fs laser pulses typically lasts a few tens of femtoseconds (*18*, *19*) and exhibits a quasi-periodic substructure of attosecond spikes at the highest (cut-off) harmonic photon energies (*12*, *20*). The spectrum of this radiation consists of discrete lines at odd multiples of the laser frequency as a spectral manifestation of temporal periodicity with a period of $T_0/2$. In the absence of a notable frequency dependence of the spectral phase, the overall emission time is related to the line width of the individual harmonics, whereas the duration of individual spikes is determined by the overall spectral width of the band of lines filtered out of the harmonic spectrum. The cut-off harmonics of a few-cycle light pulse were predicted to merge into a continuum, forming an isolated sub-femtosecond pulse (*21*–*24*). This was confirmed in a recent experiment (*9*). We demonstrate that the transition from a quasi-periodic emission with a temporal extension $\geq T_0$ to a single-pulsed sub-femtosecond emission can be continuously controlled with the pump intensity in a few-cycle–driven high-harmonic source.

Figure 3 depicts high-harmonic spectra emitted from a neon gas source pumped by 7-fs, 750-nm linearly polarized laser pulses (*8*, *9*, *25*) for a range of laser peak intensities. For the highest peak intensity the spectrum consists of well-resolved harmonic lines. Their line width implies an emission time of $\geq T_0$, i.e., the appearance of at least a couple of satellite pulses spaced by $T_0/2$ from the main pulse. Reducing the pump intensity results in harmonics merging to a continuum within the high-reflectance band (85 to 100 eV) of our Mo/Si multilayer (dashed line in Fig. 3), implying emission in a single pulse of potentially sub-femtosecond duration. The continuum portion of the few-cycle–generated harmonic spectrum is predicted to originate from driver pulses with $\varphi \approx 0$ or π, which give rise to a substantially higher peak tunneling current and, hence, dipole acceleration in the cut-off region as compared to $\varphi \approx \pm\pi/2$ for laser pulse durations approaching T_0 (*13*, *23*, *24*).

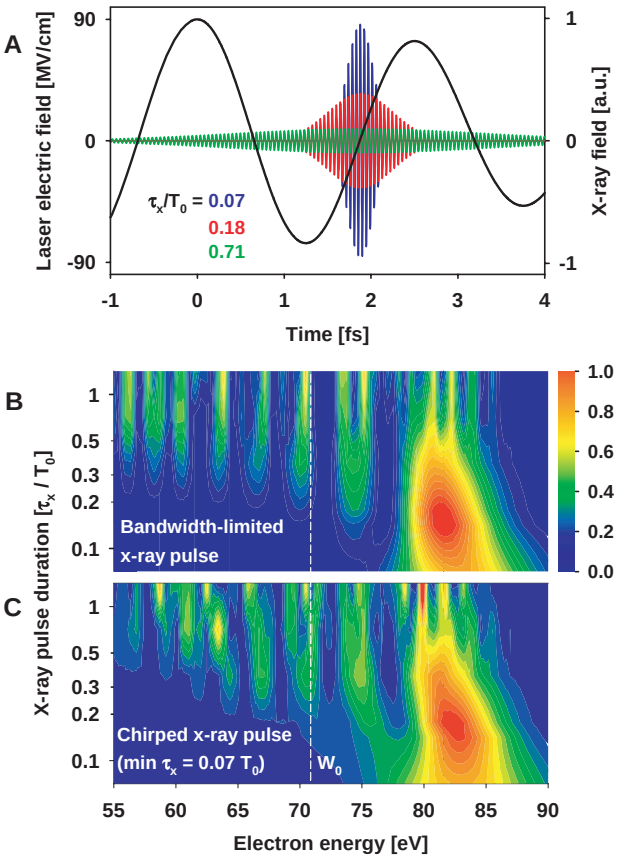

Fig. 1. Computed energy distributions of 2p photoelectrons detached from neon atoms (W_b = 21.5 eV) by a 93-eV, soft x-ray pulse in the presence of a strong 7-fs, 750-nm few-cycle light pulse for different x-ray pulse durations τ_X (contour plots; the electron yield increases from the blue to the red) using the quantum theory presented in (*11*). The electrons are detected within an infinitesimally small cone with its axis aligned parallel to the electric field vectors of the linearly polarized x-ray and laser fields (**A**). The x-ray pulse is timed to peak at the zero transition of the laser electric field. The duration of the Gaussian x-ray pulse has been varied by changing the spectral width (**B**) or by imposing a quadratic phase of variable magnitude on the spectrum (**C**). The white dashed line at $W_0 = \hbar\omega_X - W_b \approx 71$ eV indicates the position of the peak of the photoelectron spectrum in the absence of the laser field.

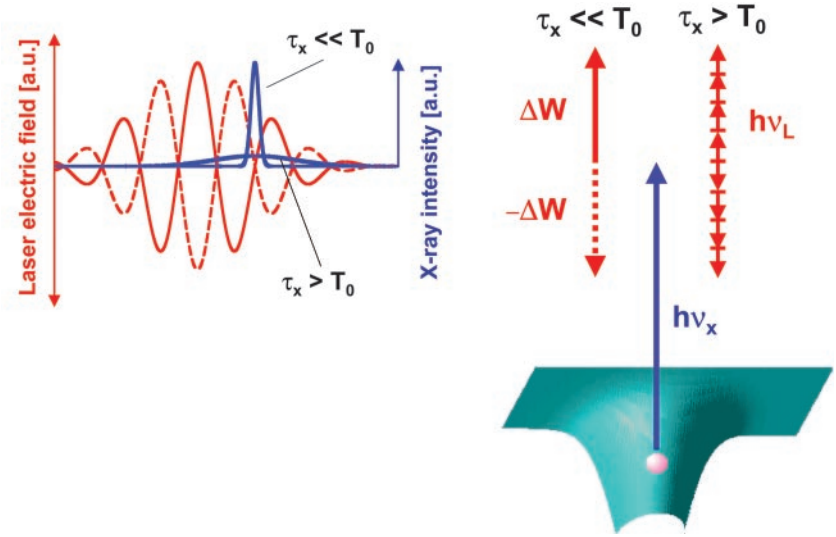

Fig. 2. Influence of a strong, linearly polarized laser field on the final energy distribution of x-ray–induced photoelectrons detected along the laser polarization as a function of the x-ray pulse duration τ_X relative to the wave cycle of the laser T_0.

Acceleration of Electron Wave Packets with Light

The harmonic beam and its pump laser beam propagate collinearly down a 2-m-long evacuated beamline to hit a concave spherical Mo/Si multilayer mirror (radius of curvature, 7 cm) at near normal incidence. The mirror has high reflectivity within a 15-eV band centered at 93 eV (see dashed line in Fig. 3) and over the entire spectrum of the sub–10-fs laser pulse, and it focuses the two collinear beams into a neon gas jet effusing from a metal-coated glass tube (inner diameter, 50 μm). The laser pulse intensity was restricted to values insufficient for laser-induced ionization. The photoelectrons produced by x-ray photons were collected within a narrow cone aligned parallel to the laser and x-ray polarization. The detection cone was defined by the 5-cm-diameter microsphere-plate detector placed 40 cm from the neon target to allow a time-of-flight analysis of the photoelectrons. The x-ray beam spot size in the target was more than an order of magnitude smaller than that of the laser beam, ensuring that all the x-ray photoelectrons were exposed to the same light field.

Before hitting the Mo/Si mirror, the beams are passed through an aperture of adjustable diameter (iris), which was used for fine adjustment of the laser pulse intensity in the neon target. The iris selected near-axis rays within a diameter of ≤3 mm of the laser beam of several centimeters in diameter. The transmitted laser beam had a nearly flat-top intensity profile, implying a quadratic and linear scaling of focused intensity and electric field E_L, respectively, with transmitted pulse energy in the photoionization region. By varying the iris diameter and monitoring the transmitted pulse energy, we could therefore accurately control relative changes of E_L in the interaction volume.

Figures 4 and 5 display electron energy spectra as a function of the measured relative change of E_L in a false-color representation. In the absence of a light field, the photoelectron energy spectrum (lowest plot on the right of Fig. 5) mimics that of the x-ray pulse downshifted by the ionization potential of neon (W_b = 21.5 eV). Figure 4 reveals a spread of electron energies rapidly increasing with increasing laser field strength when photoionization is performed using a train of x-ray pulses with spectrum a in Fig. 3. The data depicted in Fig. 5 have been collected with x-ray pulses having a continuous spectrum. In contrast to the behavior shown in Fig. 4, with increasing field strength the electron energy spectrum is upshifted as a whole without a dramatic distortion of its shape. This indicates that the x-ray pulse is of sub-femtosecond duration and is emitted at the zero transition of the driving laser electric field from the harmonic source (*26*), in accordance with numerical simulations (*9*). The simultaneous appearance of an up- and down-shifted spectral feature is the consequence of pump pulses with $\varphi \approx 0$ and $\varphi \approx \pi$ contributing to the electron spectra accumulated over many laser shots, i.e., of the lack of phase stabilization of our sub–10-fs laser pulses.

Figure 5 reveals the linear dependence of the energy shift on E_L, corroborating the prediction of our simple classical analysis. The measured spectra can be well reproduced by simulating the electron wave packet as a classical ensemble of electrons distributed across initial energies and release times whose motions are governed by the laws of classical physics. Approximating the initial energy distribution with a Gaussian function (bottom red line in Fig. 5) and assuming a bandwidth-limited x-ray pulse ($\tau_x \approx 0.2$ fs) that peaks at $E_L(t_r) = 0$, the classical and the quantum analysis delivers results (central and upper red lines in Fig. 5) in good agreement with the spectra measured for different strengths of $E_a(t_r)$. Attosecond confinement appears to mask quantum effects in the interaction of electrons with light.

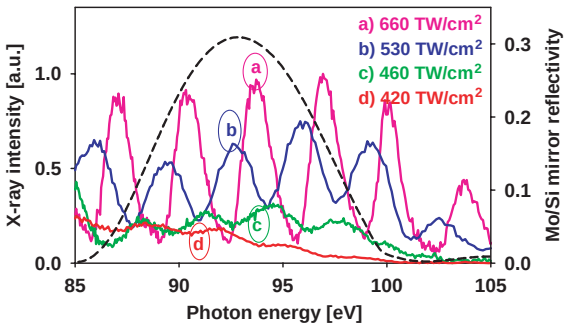

Fig. 3. High-order harmonic spectra emitted from a 2-mm-long, 110-mbar neon gas source exposed to linearly polarized 7-fs, 750-nm laser pulses with peak intensities given in the figure. Dashed line, reflectance curve of the broadband Mo/Si multilayer mirror used to select radiation for the photoionization experiments, as calculated using data from in situ measurements of the roughness and thickness of the Mo and Si layers. The reflectivity band extends over some 15 eV with a FWHM of ≈ 9 eV.

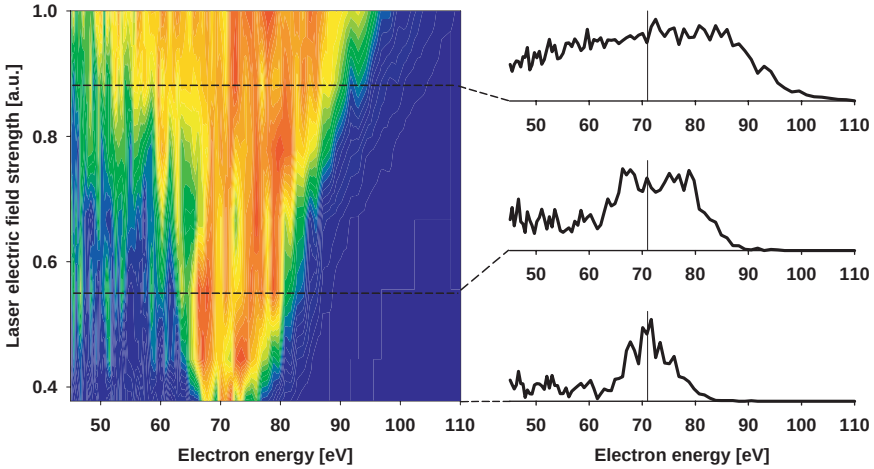

Fig. 4. Photoelectron spectra generated at different light field strengths by a sequence of sub-femtosecond soft x-ray pulses. The peak intensity of the laser pulse driving the harmonics was adjusted to 650 to 700 TW/cm² to produce a discrete harmonic spectrum (see Fig. 3) within the range of 85 to 100 eV with a duration of the pulse train of $\geq T_0$.

Attosecond Diagnostics

The generation of isolated sub-femtosecond x-ray pulses synchronized to a strong few-cycle light pulse (*9*) opens up a route to time-resolved (pump-probe) inner-shell atomic spectroscopy by using the x-ray pulse as a pump and the light pulse as a probe (*13*). Indispensable to the routine application of this new tool is a reliable, simple, and fast diagnostic test of its key characteristics. These include the strength and phase-stability of the few-cycle probe field, the timing jitter between the x-ray pulse and light wave, and the duration of the x-ray pulse. The sensitivity of the energy spectrum of the x-ray–induced, light-accelerated photoelectrons to these parameters makes it an ideal diagnostic tool for attosecond spectroscopy.

Strength and phase stability of the few-cycle probe light field. Because of the favorable timing of the sub-femtosecond harmonic pulse to its few-cycle driver, which satisfies $E_L(t_r) \approx 0$, the photoelectron energy shift in Fig. 5 directly probes the instantaneous electric field amplitude $E_a(t_r)$ with an accuracy of better than 10%. This provides direct experimental access to the peak electric field strength of an intense light pulse. Moreover, the light-accelerated electron

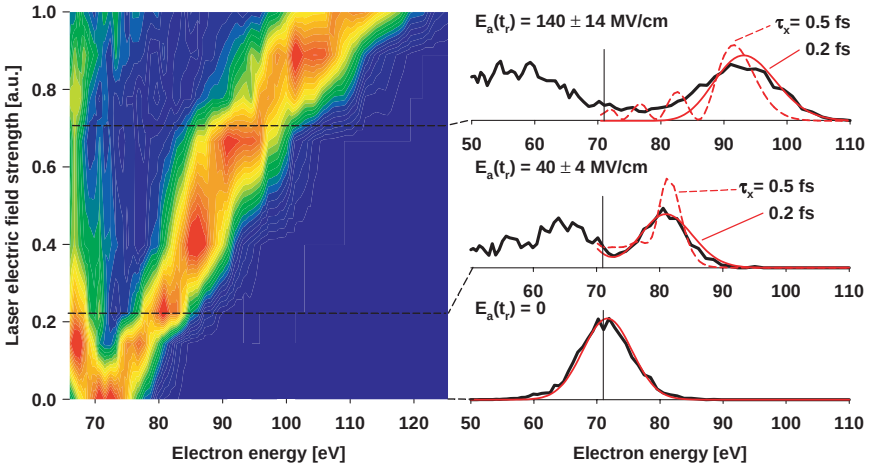

Fig. 5. Photoelectron spectra generated at different light field strengths by an isolated sub-femtosecond x-ray pulse. The peak intensity of the laser pulse driving the harmonics was adjusted in the range of 400 to 450 TW/cm^2 to generate a continuous harmonic spectrum in the 85- to 100-eV spectral range (Fig. 3). $E_L(t_r)$ has been evaluated from the observed energy shift. The bottom red line is the model x-ray spectrum (downshifted by the electron binding energy of 21.5 eV) used in the simulations resulting in the central and upper red lines for bandwidth-limited 0.2-fs (solid lines) and 0.5-fs soft x-ray pulses carrying a quadratic spectral phase (dashed lines).

proves a sensitive probe of the absolute-phase stability of intense few-cycle light. If φ is firmly locked to zero, the photoelectrons would be exclusively accelerated (with the convention of $E_L > 0$ implying a field vector that points toward the electron detector). This would imply a disappearance of the downshifted spectral feature, offering a reliable diagnostics of the phase stability of intense few-cycle pulses (*27*) for future phase-stabilized systems.

Timing jitter between the x-ray pulse and the probe light phase. Jitter affects the temporal resolution to the same extent as τ_x and T_0 (*13*); therefore, its measurement is imperative for attosecond spectroscopy. The periodic harmonic structure can be perceived in several downshifted spectra (*28*), e.g., in the central plot in Fig. 5 (the structure tends to get blurred in the upshifted features because of time-of-flight resolution worsening for increasing electron energy). Resolving the harmonic structure in energy-shifted spectra results in an upper limit of ±10% of the energy shift on smearing of the electron spectrum (accumulated over many laser shots) due to fluctuations in $E_L(t_r)$ by either laser intensity variations or x-ray pulse timing jitter. This yields a shot-to-shot timing stability of the x-ray pulse to the phase of its few-cycle driver of better than ±0.2 fs (*29*).

X-ray pulse duration. Figures 4 and 5 confirm that the energy spectrum of the light-accelerated x-ray photoelectron responds sensitively to temporal broadening of the ionizing x-ray pulse. Although a conspicuous energy spread is predicted to come into play only as τ_x becomes longer than $T_0/3$ (Fig. 1C), a considerable narrowing of the energy-shifted spectral feature already sets in for $\tau_x > T_0/10$. We calculated the light-accelerated photoelectron spectra for chirped x-ray pulses by assuming a quadratic as well as higher-order spectral phase. The root-mean-square deviation of the calculated spectra from the measured ones was a minimum for near-bandwidth–limited pulses of $\tau_x \approx 0.2$ fs (solid red lines in Fig. 5) and was increased by more than a factor of three for chirped pulses with $\tau_x \geq 0.5$ fs (*30*). Considering the minor role of spectral smearing effects, our analysis yields a safe upper limit of $\tau_x \leq 0.5$ fs for the x-ray pulse duration.

Conclusions

Photoelectron wave packets excited by an x-ray pulse within a time interval of several hundred attoseconds can be efficiently accelerated or decelerated by the electric field of light. The sensitivity of the final energy distribution of the electron to (i) the strength and (φ dependent) sub-cycle evolution of the light field, (ii) the timing of the x-ray pulse with respect to the light phase, and (iii) the sub-femtosecond temporal structure of the x-ray pulse permits reliable measurement of the key parameters of an attosecond pump-probe apparatus based on a sub-femtosecond x-ray pulse synchronized to a strong few-cycle light wave (*13*). These measurements consume orders of magnitude less time and can be performed with a much simpler apparatus as compared to the previous implementation of time-domain attosecond metrology (*9*). The substantially enhanced electron yield and larger variation of the electron spectrum owing to detection parallel to the x-ray and laser polarization (*11*), respectively, hold out the promise of sub–100-as resolution in the measurement of the x-ray pulse duration and timing jitter. However, the potential of this attosecond diagnostics can be fully exploited only with phase-stabilized few-cycle light. With φ stabilized, both the fractional energy carried by possible satellites (*11*) and the chirp (*10*) of the sub-femtosecond x-ray pulse can be determined. Accurate chirp measurements will be a key to the reliable generation of sub–100-as x-ray pulses.

References and Notes

1. A. Weingartshofer, J. K. Holmes, G. Caudle, E. M. Clarke, H. Krüger, *Phys. Rev. Lett.* **39**, 269 (1977).
2. R. R. Freeman, P. H. Bucksbaum, *J. Phys. B.* **24**, 325 (1991).
3. J. M. Schins *et al.*, *Phys. Rev. Lett.* **73**, 2180 (1994).
4. T. E. Glover, R. W. Schoenlein, A. H. Chin, C. V. Shank, *Phys. Rev. Lett.* **76**, 2468 (1996).
5. This applies in the nonrelativistic limit for interaction times short enough to prevent the electron from traveling distances comparable to or larger than the light wavelength during the interaction (dipole approximation). These conditions are fulfilled by femtosecond pulses of visible light at intensities below 10^{18} W/cm^2. In this intensity regime of interactions, ponderomotive effects provide the only means of affecting electron motion by light. For ultrashort (<1 ps) pulse durations, electrons released into a strong field lose energy equal to the ponderomotive potential of the laser, which is transferred into a blue shift of the radiation (*6*). The ponderomotive potential of long pulses, on the other hand, is capable of modifying the momentum of free electrons (*7*).
6. E. Yablonovits, *Phys. Rev. Lett.* **60**, 795 (1988).
7. P. H. Bucksbaum, M. Bashkansky, T. J. McIlrath, *Phys. Rev. Lett.* **58**, 439 (1987).
8. M. Drescher *et al.*, *Science* **291**, 1923 (2001).
9. M. Hentschel *et al.*, *Nature* **414**, 509 (2001).
10. J. Itatani *et al.*, *Phys. Rev. Lett.* **88**, 173903 (2002).
11. M. Kitzler, N. Milosevic, A. Scrinzi, F. Krausz, T. Brabec, *Phys. Rev. Lett.* **88**, 173904 (2002).
12. P. M. Paul *et al.*, *Science* **292**, 1689 (2001).
13. F. Krausz, *Opt. Photon* **13**, 62 (2002).
14. In our detection geometry, only electrons that are ejected with zero velocity in the direction orthogonal to the detection cone can be observed. These electrons experience only acceleration or deceleration by the field without any change in the direction of their momentum. However, electrons with nonzero transversal velocity component are also ejected. These electrons are indeed steered because the laser field changes the direction of their motion. They could be observed by aligning the detection cone so that it forms a nonzero angle with the laser electric field vector.
15. Control of the electron's drift velocity could be previously accomplished by using a microwave field [D. A. Tate, D. G. Papaioannou, T. F. Gallagher, *Phys. Rev. A* **42**, 5703 (1990)].
16. A. L'Huillier, P. Balcou, *Phys. Rev. Lett.* **70**, 774 (1993).
17. J. J. Macklin, J. D. Kmetec, C. L. Gordon III, *Phys. Rev. Lett.* **70**, 766 (1993).
18. Y. Kobayashi, T. Sekikawa, Y. Nabekawa, S. Watanabe, *Opt. Lett.* **23**, 64 (1998).
19. E. S. Toma *et al.*, *Phys. Rev. A* **62**, 061801(R) (2000).
20. N. A. Papadogiannis, B. Witzel, C. Kalpouzos, D. Charalambidis, *Phys. Rev. Lett.* **83**, 4289 (1999).
21. I. P. Christov, M. M. Murnane, H. C. Kapteyn, *Phys. Rev. Lett.* **78**, 1251 (1997).
22. C. Kan, N. H. Burnett, C. E. Capjack, R. Rankin, *Phys. Rev. Lett.* **79**, 2971 (1997).
23. A. de Bohan, P. Antoine, D. B. Milosevic, B. Piraux, *Phys. Rev. Lett.* **81**, 1837 (1998).
24. T. Brabec, F. Krausz, *Rev. Mod. Phys.* **72**, 545 (2000).
25. M. Schnürer *et al.*, *Phys. Rev. Lett.* **83**, 722 (1999).
26. The harmonic spikes in the train corresponding to spectrum a in Fig. 3 are also predicted to emerge near the zero transition of the driving laser electric field. As a consequence, only an up- and downshifted spectral feature would be expected, if the spikes were not longer than $T_0/5$ and the probe field $E_L(t)$ would be perfectly periodic. A blue shift near the laser pulse peak [induced by ionization in the harmonic generation process; see (*9*)], however, impairs synchronism between the x-ray pulse sequence and the zero transitions of the probe laser field. In addition, the spikes

are predicted to carry a substantial chirp and, hence, to be broadened in the "plateau" region.
27. G. G. Paulus *et al.*, *Nature* **414**, 182 (2001).
28. Note that tiny variations in the peak laser intensity can make the harmonic structure more or less pronounced as revealed by spectra c and d in Fig. 3. However, the modulation depth was kept below 25% in all measurements shown in Fig. 5, resulting in negligible fractional satellite energy content.
29. It is important to emphasize that this timing stability may not be valid for arbitrary values of the absolute phase φ of the driver pulse because laser shots characterized by a φ considerably deviating from 0 or π are expected to deliver only a small contribution to energy-shifted spectral features. As a consequence, the evaluated upper limit on the timing jitter applies to laser pulses with $\varphi \approx 0$ or π only.
30. This finding is in accordance with our recent measurement (*9*) resulting in almost zero phase distortion over the 5-eV bandwidth (FWHM) of the subfemtosecond harmonic pulse generated under similar experimental conditions in the same spectral range.
31. The theory used extensively in this work (*11*) was developed under the guidance of T. Brabec. The transmission-grating x-ray spectrograph was provided by T. Wilhein and by G. Schmahl. The computer-controlled data acquisition system was significantly improved by M. Hornung. We had illuminating discussions with G. Reider. All contributions are gratefully acknowledged. Sponsored by the Fonds zur Förderung der Wissenschaftlichen Forschung in Österreich (Austria, grants Y44-PHY and F016), the Deutsche Forschungsgemeinschaft (Germany, grants SPP1053, HE1049/9, and KL1077/1), and the European Union's Human Potential Programme under contract HPRN-2000-00133 (Atto).

13 May 2002; accepted 1 July 2002
Published online 11 July 2002;
10.1126/science.1073866
Include this information when citing this paper.

REPORTS

Imaging Quasiparticle Interference in $Bi_2Sr_2CaCu_2O_{8+\delta}$

J. E. Hoffman,[1] K. McElroy,[1] D.-H. Lee,[1,6] K. M Lang,[1,2] H. Eisaki,[3,4,5] S. Uchida,[5] J. C. Davis[1,6]*

Scanning tunneling spectroscopy of the high-T_c superconductor $Bi_2Sr_2CaCu_2O_{8+\delta}$ reveals weak, incommensurate, spatial modulations in the tunneling conductance. Images of these energy-dependent modulations are Fourier analyzed to yield the dispersion of their wavevectors. Comparison of the dispersions with photoemission spectroscopy data indicates that quasiparticle interference, due to elastic scattering between characteristic regions of momentum-space, provides a consistent explanation for the conductance modulations, without appeal to another order parameter. These results refocus attention on quasiparticle scattering processes as potential explanations for other incommensurate phenomena in the cuprates. The momentum-resolved tunneling spectroscopy demonstrated here also provides a new technique with which to study quasiparticles in correlated materials.

In an ideal metal, the Landau-quasiparticle eigenstates are Bloch wavefunctions characterized by wavevector $\vec{k}$ and energy ε. Their dispersion relation, $\varepsilon(\vec{k})$, can be measured with momentum-resolved techniques such as angle-resolved photoemission spectroscopy (ARPES). By contrast, real space imaging techniques, such as scanning tunneling microscopy (STM), cannot be used to measure $\varepsilon(\vec{k})$. This is because the local-density-of-states LDOS(E) spectrum at a single location $\vec{r}$ is related to the $\vec{k}$-space eigenstates $\psi_k(\vec{r})$ by

$$\mathrm{LDOS}(E,\vec{r}) \propto \sum_k |\psi_k(\vec{r})|^2 \delta(E - \varepsilon(\vec{k})) \quad (1)$$

and substitution of a Bloch wavefunction into Eq. 1 shows LDOS(E) to be spatially uniform.

When sources of disorder such as impurities or crystal defects are present, elastic scattering mixes eigenstates that have different $\vec{k}$ but are located on the same quasiparticle contour of constant energy (CCE) in $\vec{k}$-space. When scattering mixes states $\vec{k}_1$ and $\vec{k}_2$, an interference pattern with wavevector $\vec{q} = \vec{k}_2 - \vec{k}_1$ appears in the norm of the quasiparticle wavefunction and LDOS modulations with wavelength $\lambda = 2\pi/|\vec{q}|$ appear. These phenomena can be observed by STM as modulations of the differential tunneling conductance, which are often (imprecisely) referred to as "Friedel oscillations." STM studies of such conductance modulations have allowed the first direct probes of the quantum interference of electronic eigenstates in metals and semiconductors (*1*–*5*).

The Bogoliubov-quasiparticles in a Bardeen-Cooper-Schrieffer superconductor are also Bloch states but with dispersion

$$E_{\pm}(\vec{k}) = \pm\sqrt{\varepsilon(\vec{k})^2 + \Delta(\vec{k})^2} \quad (2)$$

where $|\Delta(\vec{k})|$ is the $\vec{k}$-dependent magnitude of the energy gap at the Fermi surface (CCE for $\varepsilon(\vec{k}) = 0$ in the normal state). Elastic scattering of Bogoliubov-quasiparticles can also result in conductance modulations. Quasiparticle standing waves have been imaged by STM in the conventional superconductor Nb (*6*) and in the CuO chains of YBCO (*7*). For the cuprates in general, it has long been proposed that conductance modulations due to quasiparticle scattering should occur, and that both the homogeneous electronic structure and superconducting gap anisotropy could be extracted from measurement of their properties (*8*).

When LDOS modulations are detected by STM in a given sample, certain CCE in $\vec{k}$-space can be reconstructed by analyzing the Fourier transform of the real-space LDOS(E) image (*3*, *9*, *10*). This is potentially a powerful technique because, for any

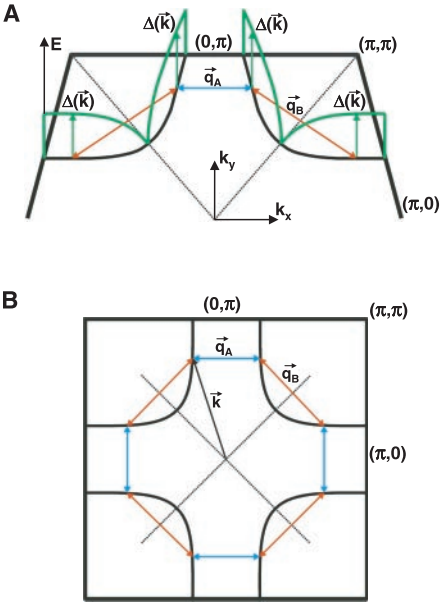

Fig. 1. (**A**) A perspective view of the superconducting energy gap Δ (green) as a function of the location along the Fermi surface (black). (**B**) Schematic Fermi surface of Bi-2212. Vectors connecting the eight areas of the Fermi surface with identical $|\Delta|$ are shown and labeled by blue and red arrows depending on the type of elastic scattering process at $E = |\Delta|$ that connects them.

[1]Department of Physics, University of California, Berkeley, CA 94720–7300, USA. [2]Electromagnetic Technology Division, National Institute of Standards and Technology, Boulder, CO 80305–3328, USA. [3]Department of Applied Physics, Stanford University, Stanford, CA 94305–4090, USA. [4]Agency of Industrial Science and Technology, 1-1-1 Central 2, Umezono, Tsukuba, Ibaraki, 305-8568 Japan. [5]Department of Superconductivity, University of Tokyo, Tokyo, 113-8656 Japan. [6]Materials Sciences Division, Lawrence Berkeley National Laboratory, Berkeley, CA 94720, USA.

*To whom correspondence should be addressed. E-mail: jcdavis@socrates.berkeley.edu